Experimental insights into pyroclast-ice heat transfer in water-drained, low pressure cavities during subglacial explosive eruptions

D C Woodcock, S J Lane and J S Gilbert

Lancaster Environment Centre, Lancaster University, Lancaster LA1 4YQ, UK

d.woodcock@lancaster.ac.uk

Abstract

Subglacial explosive volcanism generates hazards that result from magma-ice interaction, including large flowrate meltwater flooding and fine-grained volcanic ash. We consider eruptions where subglacial cavities produced by ice-melt during eruption establish a connection to the atmosphere along the base of the ice sheet that allows accumulated meltwater to drain. The resulting reduction of pressure initiates or enhances explosive phreatomagmatic volcanism within a steam-filled cavity with pyroclast impingement on the cavity roof. Heat transfer rates to melt ice in such a system have not, to our knowledge, been assessed previously. To study this system, we take an experimental approach to gain insight into the heat transfer processes and to quantify ice-melt rates. We present the results of a series of analogue laboratory experiments in which a jet of steam, air and sand at approximately 300 °C impinged on the underside of an ice block. A key finding was that, as the steam to sand ratio was increased, behavior ranged from predominantly horizontal ice melting to predominantly vertical melting by a mobile slurry of sand and water. For the steam to sand ratio that matches typical steam to pyroclast ratios during subglacial phreatomagmatic eruptions at c. 300 °C we observed predominantly vertical melting with upward ice-melt rates of 1.5 mm s^{-1}, which we argue is similar to that within the volcanic system. This makes pyroclast-ice heat transfer an important contributing ice-

melt mechanism under drained, low pressure conditions that may precede subaerial explosive volcanism on sloping flanks of glaciated volcanoes.

1 Introduction

Subglacial eruptions generate hazards that result from the interaction of magma with ice. Fragmentation of magma may promote efficient magma-ice heat transfer [*Gudmundsson et al.*, 2004]. The consequent release of large flowrates of meltwater, together with mobilization of volcanic sediments, has the potential for both infrastructure damage and loss of life [*Bird et al.*, 2010]. Subglacial eruptions may penetrate the overlying ice by a combination of upward melting and fracturing to become subaerial [*Gudmundsson*, 2005]. The resulting volcanic plumes present a variety of proximal to distal hazards. In particular, interaction of magma with meltwater may produce fine-grained ash that disperses widely in the atmosphere, leading to local deposition hazard together with restrictions on air traffic and subsequent disruption to global air travel and supply chains [*Dellino et al.*, 2012; *Harris et al.*, 2012].

Rates of ice melt are determined by eruption rates together with the rate at which the initial heat content of the magma is transferred to the ice. We consider a subglacial fissure eruption which melts a cavity in the ice that subsequently drains by connection to the atmosphere along a conduit at the base of the ice sheet. On drainage, reduction of pressure at the vent enhances or initiates magmatic and/or phreatomagmatic explosivity to produce a buoyant jet of steam and pyroclasts. Such cavities are expected to be vapor-dominated, with steam sourced principally from phreatomagmatic activity [*Wilson and Head,* 2002; *Woodcock et al*., 2016]. Cavity pressure is expected to be near atmospheric, with meltwater drained by gravity and the elevation of cavity pressure above atmospheric determined by frictional and accelerational pressure losses associated with the removal of excess fluid.

Figure 1 shows a schematic cross section of a water-drained, low pressure ice cavity containing a buoyant eruption jet of steam and pyroclasts that emerges from the vent. Initial jet momentum and developing plume buoyancy force steam and pyroclasts to impinge on the ice cavity roof. On either side of the buoyant jet, the cavity contents circulate in turbulent forced convection driven by momentum transfer from the jet. This flow comprises steam, together with the smaller pyroclasts that tend to follow the fluid streamlines. We envisage heat transfer to the overlying ice from the buoyant jet and the cavity contents by a combination of forced convective steam condensation and, where pyroclasts contact the ice surface, by pyroclast-ice heat transfer across fluid contact films. The resulting vertical ice-melt rate is the main control on the time taken for an eruption to breach the surface. At this point, thermal coupling with the atmosphere begins with concomitant reduction in total ice melt-rate.

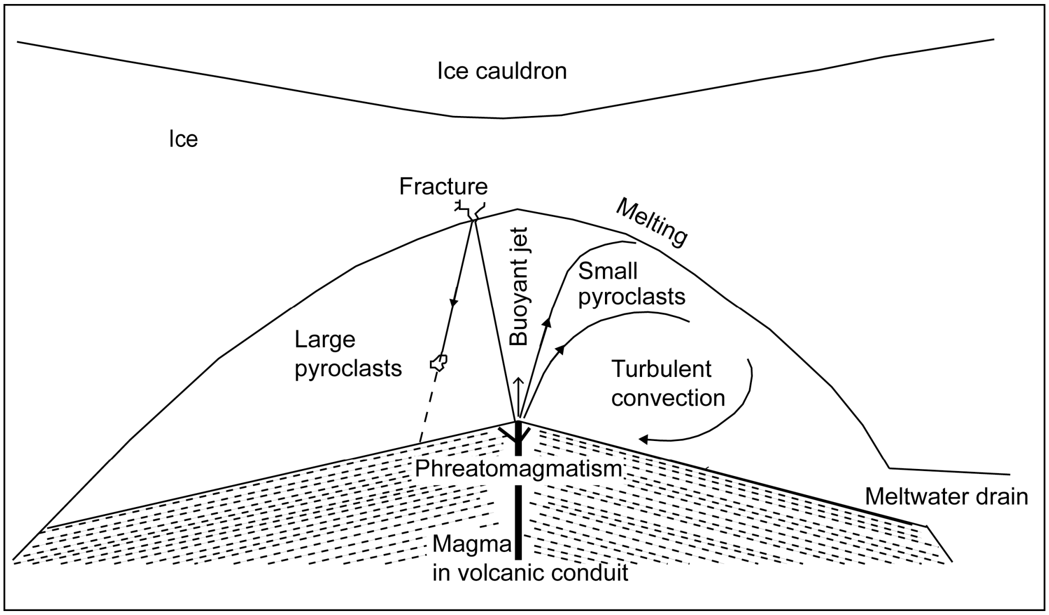

Figure 1. Schematic diagram of a vapor-dominated ice cavity, produced during a subglacial eruption. This cavity drains meltwater continuously and is depressurized by connection to the atmosphere to allow the formation of a buoyant eruption jet of steam and pyroclasts. Heat transfer from the explosive eruption to the ice is by a combination of steam condensation and direct particle-ice heat transfer. On the left hand side of the figure, large pyroclasts travel on ballistic trajectories and rebound from the roof on impact, thus they transfer negligible heat but may fracture the ice. On the right hand side of the figure, small pyroclasts follow fluid streamlines and transfer much of their heat directly to the ice surface or indirectly by convection to the cavity steam.

Heat transfer during the impingement of hot pyroclasts onto ice during subglacial explosive eruptions has not, to our knowledge, been studied previously. We address the knowledge gap through an experimental approach in order to gain insight into the behavior of a buoyant jet of pyroclasts when it interacts with a downward-facing ice surface and to determine heat transfer rates for comparison with other plausible ice-melt mechanisms in subglacial eruptions. In Sections 2 and 3 we report analogue experiments in which hot quartz sand impinges the underside of ice blocks and the resulting cavity development is studied. In Section 4 we discuss the relevance of the experiments to volcanic systems in nature.

2 Method

2.1 Scaling between eruption and experiment

During explosive subglacial eruptions we expect that growth of an ice cavity will be dependent on pyroclast flux and the ratio of the initial cavity width to the eruption jet width, together with pyroclast size, velocity and temperature. Where there is significant magma-water interaction in the conduit, pyroclast temperature will be reduced with thermal energy redistributed into vaporizing water, thus the steam to pyroclast ratio becomes an important control as well as pyroclast temperature. Table 1 lists the values of variables typical for explosive subglacial eruptions in water-drained, low pressure cavities that were used to develop the experimental approach. Several variables, or ratios of variables, have values in the experiments that are similar to those characteristic of subglacial eruptions; however, in common with all complex systems, analogue scaling was a compromise requiring interpretation.

We expect pyroclast size to be the dominant control on the extent of pyroclast-ice heat transfer [*Gudmundsson*, 2003]. Large pyroclasts travel ballistically, are likely to rebound on impact, and are unlikely to be captured by surface tension, giving contact times that are short compared with cooling times (Figure 1). Large pyroclasts will thus transfer minimal heat to the ice surface unless they break into smaller particles on impact, but may cause significant mechanical impact damage to the ice surface. Small pyroclasts that interact with the ice are less likely to rebound on impact with the

Table 1. Comparison of values of variables in the experiments with values typical for subglacial eruptions in drained, low pressure cavities

Variable name	Value in subglacial eruption	Value in experiments	Comparison	Implication	Notes
Linear scale	Jet: 2-3 m wide[a] Cavity: 20 -100 m[b]	Jet: 6 mm diam Cavity: 6-10 cm	Scale ratio c. 10^2-10^3		Inevitable large scale ratio
Initial cavity to jet size ratio	7-50	10-17	Similar		
Heat flux in jet	300 MW m^{-2} (Gjálp 1996[c])	100 MW m^{-2}	Similar		
Particle velocity	100 m s^{-1}	50 m s^{-1}	Similar		
Particle size	0.002 - 45 mm (Gjálp1996[c])	0.1-0.5 mm	Experiments use a subset of particle size range		Experiments limited by cohesion or blocking of apparatus
Particle thermal diffusivity	c. 10^{-6} m^2 s^{-1}	c. 10^{-6} m^2 s^{-1}	Similar		
Particle temperature	700-1100 °C maximum, lower if magma-water interaction in conduit	c. 300 °C	Similar for phreatomagmatic eruption		Limited scope to increase in experiments
Ice temperature	Pressure melting point (temperate glacier)	c. -4 °C	Slight subcooling in experiments	Negligible	Impractical to use warmer ice
Cavity pressure	Atmospheric or slightly elevated	Atmospheric	Similar		For eruptions in drained, low pressure cavities
Cavity fluid (mass %)	<10 % inerts >90 % steam	70-100 % air (inerts) 0-30 % steam	Much higher inerts % in experiments	Steam condensation heat transfer coefficient lower in experiments	
Steam to particle mass ratio in jet	Up to 0.4[d], depending on extent of magma-water interaction in conduit	0-0.7	Similar		
Non-dimensional numbers					
Gr/Re2	4×10^{-2}	2×10^{-4}	Heat transfer by forced		See section S2.2 in

			convection in both cases		Supporting Information
Jet Re	2×10^7	2×10^4	Jet is turbulent in both cases		See section S2.3 in Supporting Information
Stokes no.[e]	0.05	25	Particles kinematically and thermally decoupled in experiment but not in subglacial eruption	Cooler and slower particles impinge on ice surface in volcanic case	See section S2.4 and S2.5 in Supporting Information
"Thermal Stokes no." [f]	0.02	10			
Ratio of cavity height to Morton length scale[g]	1	0.05	More entrainment in subglacial jet that in experimental jet	Slower particles impinge on ice surface in volcanic case	See section S2.6 in Supporting Information

[a] Based on a dyke width of c. 1 m [*Gudmundsson et al.*, 2004] and some expansion of the vent within the volcanic edifice
[b] Based on observations of minor eruptions on slopes south of the summit caldera of Eyjafjallajökull in 2010 [*Magnússon et al.*, 2012]
[c] [*Gudmundsson*, 2003]
[d] Based on basaltic magma at 1100 °C with 1 wt % magmatic steam
[e] [Raju and Meiburg, 1995]
[f] Ratio of cooling time to transit time for particles
[g] [Papanicolaou and List, 1988]

wet ice surface. We demonstrate in section S1 of the Supporting Information that ash-sized pyroclasts (< 2 mm in diameter) are likely to be retained by surface tension if they impinge on the wet ice surface. Small pyroclasts may thus have contact times that approach or exceed their cooling times, allowing efficient heat transfer between pyroclast and ice (Figure 1). Pyroclasts that are retained in the circulating interior of the cavity are cooled by convective heat transfer to the cavity steam and thus transfer heat to the ice indirectly by steam condensation [*Woodcock et al*., 2016]. Overall, it seems likely that much of the direct and indirect heat transfer between a buoyant jet of pyroclasts and an ice surface will be due to the small pyroclasts.

A particle size range of 0.1-0.5 mm was used in the experiments. This size range is narrower than that for subglacial eruptions [*Gudmundsson et al*., 2004; *Stevenson et al*., 2011]; however, our approach was to concentrate on the smaller particles, where heat transfer from particle to ice is likely to be most efficient. In the volcanic case, particles smaller than 0.1 mm have high degrees of thermal coupling similar to those in the 0.1-0.5 mm range.

We used quartz sand rather than volcanic ash in the experiments. Volcanic ash is highly variable with morphologies ranging from blocky, non-vesicular ash produced by phreatomagmatic fragmentation to highly vesicular ash produced by magmatic fragmentation [*Dellino et al*., 2012]. As well as being less variable in morphology, sand grains are more free-flowing and less susceptible to attrition, thus allowing easy transport within the experimental apparatus and reproducible experiments. The thermal properties of quartz sand are similar to those for volcanic silicates [*Incropera and DeWitt*, 1996; *Höskuldsson and Sparks*, 1997].

Volcanically, vent width is likely to be of order 3 m and initial cavity size on drainage of order 50 m. This yields a scale of order 17. Experimentally, initial jet and cavity diameters were designed at 6 mm and 10 cm to provide similarity of space for forced convection of fluid (S2.2 of Supporting Information) external to the buoyant jet.

In order to attain similarity of the jet heat flux between volcano and experiment a balance was needed between jet area at emergence, feed rate of experimental particles and jet temperature. We obtained an experimental heat flux of one third that inferred for the Gjálp 1996 eruption [*Gudmundsson et al.*, 2004] using an experimental jet velocity half that of a plausible emergence velocity of volcanic jets and a jet temperature of 300°C (please see below for temperature scaling). These values also need to be considered in the light of the conditions under which volcanic ash interacts with the melting ice surface. The emerging volcanic flow of particles and water vapor is initially a hot jet. Entrainment of cooler gas causes transition through a buoyant jet to a plume or, if buoyancy is insufficient, to a collapsing fountain. The nature of the impingement on the ice surface is likely to be more plume-like in the volcanic case and more jet-like in the experimental case (S2.6 of Supporting Information). The greater degree of the kinematic coupling of the particles in a volcanic buoyant jet suggests that a smaller proportion of ash particles will be able to impinge on the ice surface than sand grains in the experiments (S2.4 of Supporting Information); however, there are two factors that may act to reduce this difference. The jets in both scenarios are turbulent (S2.3 of Supporting Information), but the volcanic jet is likely to have a considerably higher level of turbulence increasing the potential for interaction. Volcanically, the more plume-like nature, and longer timescale of the interaction between ice and buoyant jet, suggests that there is greater opportunity for pyroclast-ice interaction than may be implied from straightforward kinematic considerations. In the volcanic case of a collapsing fountain, it is likely that the interaction with the ice surface retains considerable jet-like characteristics.

The timescales of interaction in the volcanic case are sufficient for volcanic ash to be thermally coupled to the water vapor in the buoyant jet (S2.5 of Supporting Information) that is cooling by entrainment of cavity fluid. Experimentally, timescales were much shorter and sand grains retained their heat whilst within the buoyant jet. All being equal, the consequence of this greater degree of thermal decoupling is that experimental sand will be hotter than volcanic ash at it impinges against the wet ice surface. PlumeRise [*Woodhouse et al*., 2013] modeling (S5 of Supporting Information) suggests that the temperature difference could be in the region of 100-200 K, therefore experiments were carried out at a reduced source temperature to mitigate this.

In subglacial eruptions, pyroclast temperature and steam to pyroclast ratio in the eruption jet depend principally on the degree of magma-water interaction within the volcanic conduit. This is well illustrated, for subaerial eruptions, around 5 minutes into a video clip of lava fountaining during the 1959-1960 Kilauea eruption [*US Department of the Interior*, 2007], where the magma intermittently contacts shallow groundwater. At this point the lava fountain, where pyroclast temperatures may be 700-800 °C [*Spampinato*, 2008], is transformed to an ash-laden steam jet in which pyroclast temperatures could be as low as 100 °C with much of the thermal energy of the jet contained in the latent heat of steam.

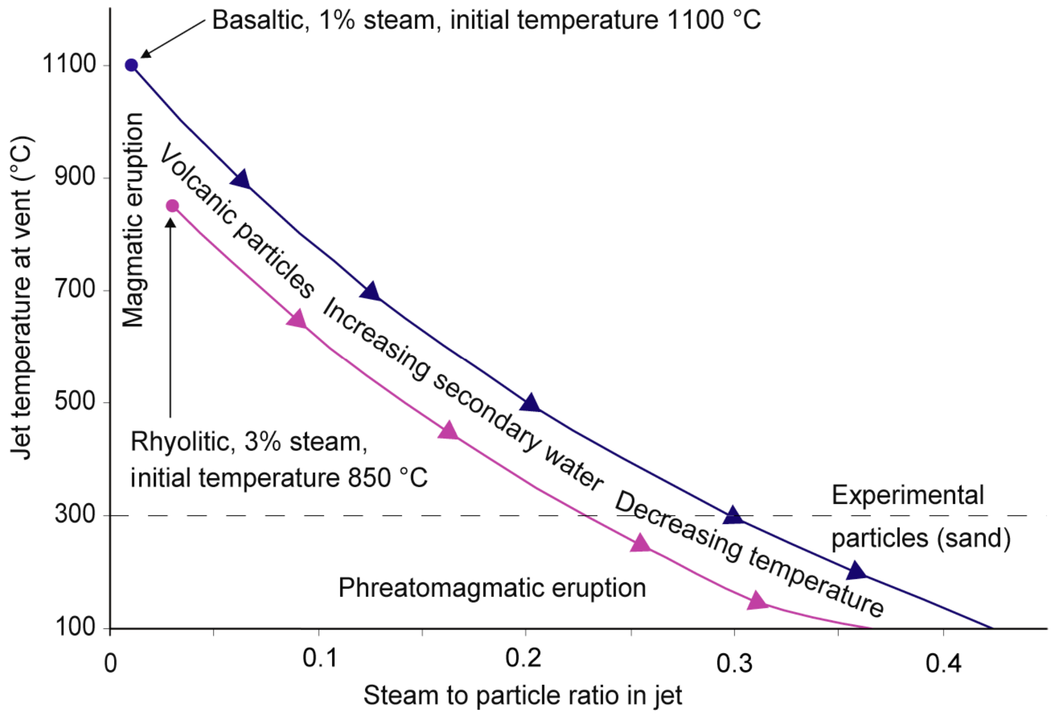

Figure 2. Steam to particle ratio in the jet, versus jet temperature, that results from increasing interaction of basaltic or rhyolitic magma with liquid water at 0 °C. Movement along the horizontal line at 300 °C represents the variation of the steam to particle (sand) ratio as the amount of steam added in our experiments was varied. In the experiments a steam to particle ratio of c. 0.2-0.3 is required to simulate a phreatomagmatic eruption at 300 °C. The figure was developed using particle specific heat capacity data from *Höskuldsson and Sparks* [1997] and enthalpy data for water from *Rogers and Mayhew* [1980].

Figure 2 shows steam to particle ratios versus thermally-equilibrated emergent jet temperatures that results from increasing interaction with liquid water at 0 °C for (1) a basaltic magma initially at 1100 °C with 1 % magmatic steam, and (2) a rhyolitic magma initially at 850 °C with 3 % magmatic steam (See section S4 in Supporting Information for the calculation). In the absence of ground water, a jet of large pyroclasts at magmatic temperature (i.e a lava fountain) is likely to form and direct heat transfer to the ice is unlikely (Figure 1). At the other extreme, the jet would have a temperature of 100°C and a water content approaching 30 % by mass. Under the water-saturated conditions likely following ice cavity drainage, a wet, warm jet of small pyroclasts and secondary steam resulting from phreatomagmatic activity between these two extremes is the most plausible explosive outcome. We scale the experiments to the temperature of a phreatomagmatic buoyant jet with 20% water (steam to particle ratio of 0.25) giving a suggested emergence temperature of 300-400 °C, depending on magma composition and initial temperature (Figure 2). For these conditions PlumeRise modelling (section S5 in Supporting Information) predicts this to produce a buoyant plume with neutral buoyancy at 690 m above the vent under cavity conditions in the volcanic case. In order to mitigate differences in thermal coupling between experiment and nature, we chose a lower experimental particle temperature of c. 300 °C. We added an appropriate flow of steam to the experimental jet to allow the simulation of phreatomagmatic eruptions. Figure 2 indicates that a steam to particle ratio in the range 0.2-0.3 is required to simulate a phreatomagmatic eruption at c. 300 °C. In addition, our ability to add steam allowed us to vary the steam to particle ratio systematically and thus to examine the effect of particle to water ratio independently of particle temperature. Movement along the horizontal line at 300 °C on Figure 2 represents the variation of the steam to particle ratio in our experiments. In order to independently vary the flow rates of sand and steam in the experimental jet we used air to convey the sand. Heat transfer from air to ice was limited by the relatively low heat transfer coefficient [*Incropera and DeWitt*, 1996]. In addition, the presence of the air halved the steam condensation heat transfer coefficient [*Woodcock et al.*, 2015] and thus enhanced the relative importance of particle-ice heat transfer.

In summary, the experimental scaling of the fluid dynamics is a balance of compromises against a volcanic system where conditions are uncertain. However, the core of the process, where heat is transferred from pyroclasts and steam in contact with a melting ice surface, is rendered similar by using materials well scaled to the volcanic case.

2.2 Experimental apparatus

Figure 3 shows a schematic diagram of part of the experimental apparatus in which hot sand particles impinged on the roof of a developing cavity in an ice block. The apparatus was constructed from copper pipe and compression fittings. Air from a screw compressor was preheated and flowed through the tee-piece at the base of the sand reservoir, where it entrained sand fed by gravity from the sand reservoir immediately above. The sand particles were accelerated in the delivery tube (1 m long, 8 mm diameter) and emerged to impinge on the underside of an ice block. Steam was fed into the delivery tube to allow the resulting steam to sand ratio in the jet to be varied.

The sand reservoir was heated by two SEI 20/50 Thermocoax® low voltage electrical heating elements attached to the outside of the sand reservoir and held in contact with thick copper wire. The air preheater, balance line and delivery tube were positioned around the sand reservoir and covered with 40-mm-thick Rocklap® rock wool insulation for heat conservation and personnel protection.

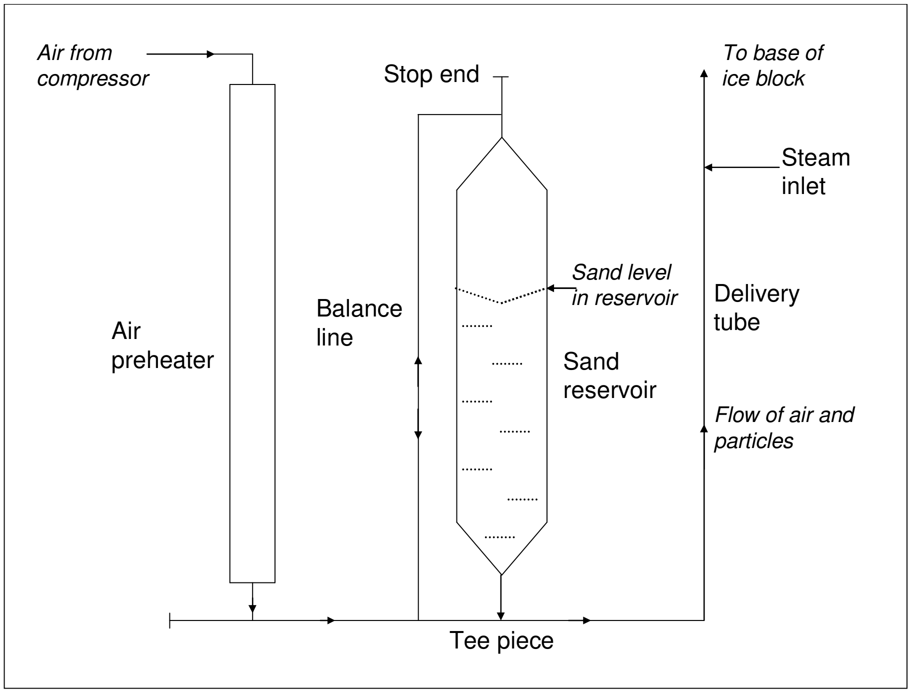

Figure 3. Schematic diagram of part of the experimental apparatus in which hot sand particles impinged on the roof of a developing cavity in an ice block. This part of the apparatus is contained within the insulation jacket in Figure 4.

The ice block was supported on a thermally insulating board with a hole and seal to allow the delivery tube exit to be positioned directly below the base of the ice block. The board allowed collection of the wet sand pile resulting from the experiment and drainage of liquid water into a separate collection pot. Figure 4 (a) shows the experimental apparatus installed in its working position.

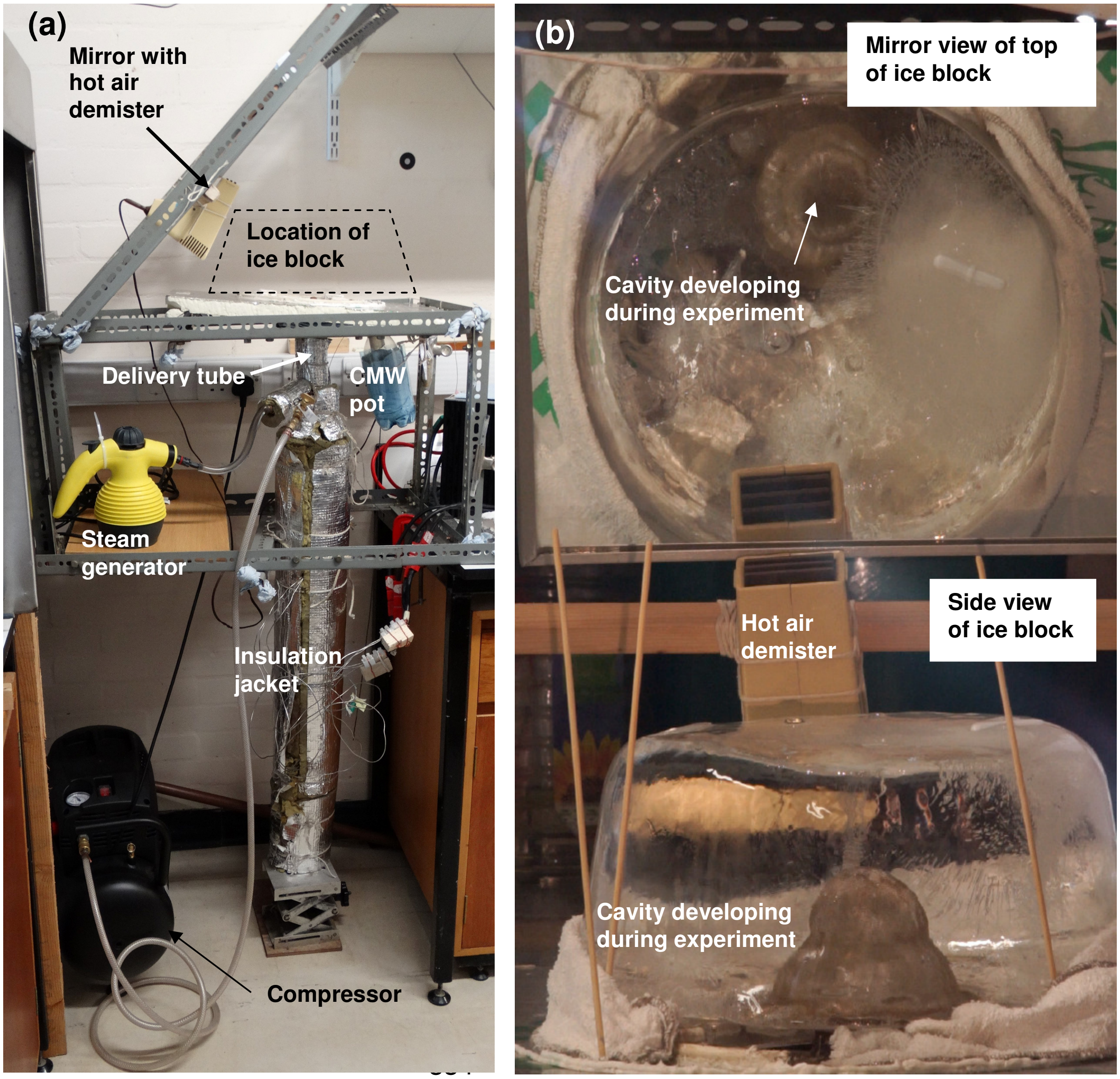

Figure 4. Overview image of the apparatus and a typical video frame collected during experiments. **(a)** The experimental apparatus installed in its working position. The location of the ice block was at approximately head height. During an experiment steam condensate plus meltwater (CMW) drained from the wet sand pile and was collected in the CMW pot. The insulation jacket (covered with silvered foil) contains the equipment shown in Figure 3. **(b)** The field of view of the video camera, showing the mirror view of the top of the ice block and the side view of the cavity that developed within a 12 cm high ice block during an experiment.

2.3 Experimental procedure

Ice blocks (10-12 cm high, 30 cm diameter) were produced from deionized, microfiltered water by slow freezing at -5 °C with continuous stirring to remove air bubbles. This ice had a density similar to glacier ice produced naturally from compacted snow [*Paterson*, 1994]. Prior to an experiment, an approximately hemispherical "preform" cavity was made in the base of the ice block to simulate the initial condition of a recently drained subglacial cavity produced during earlier stages of the eruption.

A charge of quartz sand (0.1-0.5 mm diameter particles, washed and dried) was loaded into the sand reservoir. The apparatus was heated to 350 °C and then held at constant temperature to allow any radial temperature gradient in the sand reservoir to relax. Temperature was monitored by a K-type thermocouple inserted into the delivery tube during heating. The resulting sand temperature on discharge was estimated to be c. 300 °C by a theoretical consideration of the heat transfer from the sand to the preheated conveying air during transit in the delivery tube.

When sand heating was completed the ice block was removed from the freezer, weighed and then mounted in position. The experiment was started without delay and run until the sand supply was exhausted, when air and steam were immediately stopped. Experiments were videoed at 25 frames per second and full HD (1080p) resolution (2.07 megapixels per frame) using a Sony a7 camera with a Nikon ED 180 mm f/2.8 lens. Figure 4 (b) shows a video frame of the combined mirror view and side view of the ice block during an experiment.

The ice block was returned to the freezer immediately at the end of an experiment and the temperature of the water collected was measured. The temperature of the resulting wet sand pile was measured with a thermometer at three locations in the pile and the mean of the readings was recorded. The wet sand pile was recovered from the board, weighed, dried and the resulting dry sand reweighed. The amount of ice melted was determined by weighing the ice block after the experiment. The mean sand and steam flowrates were determined from the amounts discharged at the ice block during the experiment.

As far as possible all sand discharged and all water produced were recovered. Mass balances for sand and water were carried out together with an overall heat balance after determining and applying corrections that included (1) heat ingress from the environment to the ice block during the experiment and (2) heat loss from the wet sand pile and water collected. Additional details of the experimental apparatus and procedure may be found in *Woodcock* [2016].

3 Experimental results and interpretation

3.1 Introduction

A set of 12 experiments was performed to explore the behavior of the hot sand jet, augmented by varying proportions of steam, as it impinged on an ice block. Table 2 summarizes the key results for the experiments. All experiments were carried out with the same sand, heated to c. 350 °C (c. 210 °C in Experiment 6) and discharged at the roof of an approximately 30 mm high preform cavity (Fig 5a) in an ice block with an initial temperature of -4 to -5 °C. The detailed results from each experiment are presented in the Supporting Information.

3.2 Description of experiments

In the absence of steam (Experiments 1 and 2; see Table 2), sand started to accumulate almost immediately on the roof of the preform to form a "sand cap" where the jet impinged on the ice. Sand was shed radially from the base of the cap and a thick slurry of sand and water flowed slowly in clumps down the walls of the cavity. Figure 5b shows the resulting cavity for Experiment 1, which was shallow and broad. The amount of sand discharged was the same in both experiments but the sand flowrate was three times faster in Experiment 1. The average upward melt-rate for these two experiments was c. 0.2 mm s^{-1}.

The resulting sand piles in experiments with no added steam (Experiments 1 and 2) were relatively dry with a hummocky topography. The base of the ice block around the cavity showed diffuse melting. The final temperatures of the sand pile and of the small amount of meltwater collected were in the ranges 35-40 °C and 29-30 °C respectively. Where steam was added to the jet (Experiments 3-12), the sand piles and condensate plus meltwater (CMW) were cooler and the final cavities were significantly taller and narrower than in the absence of steam.

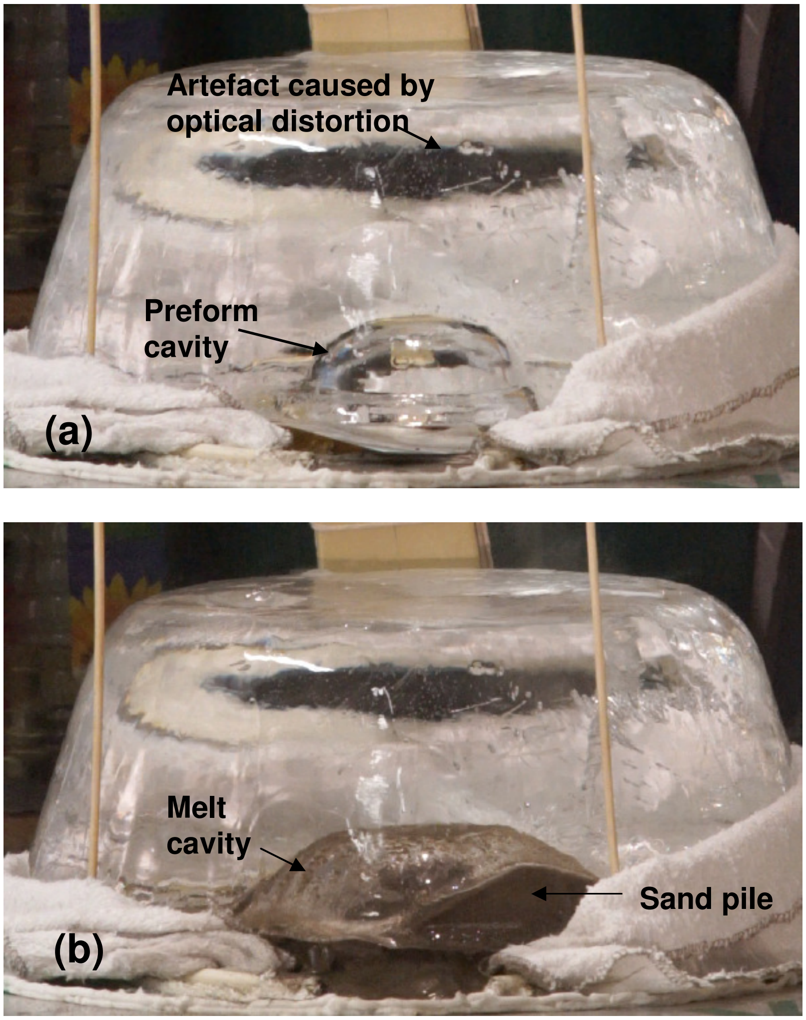

Figure 5. Individual video frames collected during Experiment 1. **(a)** A profile view of the preform cavity within the ice block at the start of the experiment. The height of the ice block from the base of the cavity to the top of the overlying ice is 11 cm. The dark area towards the top of the ice block is an artifact caused by optical distortion. (**b**) The shallow, broad cavity at the end of the experiment, showing the sand pile within the cavity.

Table 2. Summary of experimental results

Experiment number	1	2	3	4	5	6	7	8	9	10	11	12
Sand temperature[a] (+/- 2.5 °C)	336	336	332	335	334	214	336	338	333	339	332	334
Experiment duration (+/- 1 s)	30	83	34	34	54	78	65	38	78	59	54	102
Sand discharged (+/- 1 g)	294.0	291.5	299.5	199.5	173.0	200.0	200.0	100.0	200.0	200.0	100.0	50.0
Steam condensed (+/- 1 g)	0	0	14.0	13.5	19.5	28.0	24.0	14.5	29.5	40.0	28.5	39.0
Ice melted (+/- 1 g)	170	173	237	183	217	251	278	150	308	331	221	271
Sand pile temperature (+/- 1 °C)	35	40	40	29	27	19	26	28	20	29	19	16
CMW[b] temperature (+/- 0.5 °C)	30.0	29.0	28.5	26.5	21.5	20.0	20.0	20.0	19.0	21.5	17.0	18.5
Calculation of steam and sand flow rates, and steam to sand ratio												
Sand flow rate (g/s)	9.8	3.5	8.8	5.9	3.2	2.6	3.1	2.6	2.6	3.4	1.9	0.5
Steam flow rate (g/s)	0	0	0.41	0.40	0.36	0.36	0.37	0.38	0.38	0.68	0.53	0.38
Steam to sand ratio	0	0	0.05	0.07	0.11	0.14	0.12	0.14	0.15	0.20	0.29	0.78
CMW to sand ratio[b]	0.58	0.59	0.84	0.99	1.37	1.39	1.51	1.65	1.69	1.85	2.49	6.20
Ice cavity geometry, heat transfer efficiency and melt-rates												
Height of final ice cavity (+/- 1 mm)	36	50	50	72	77	74	81	64	92	102	93	107
Basal diameter of final ice cavity (+/- 1 mm)	105	95	98	84	85	85	90	81	80	82	78	77
Percentage of heat in jet transferred to ice[c]	70	74	75	75	83	90	88	88	87	85	87	99
Mean vertical melt-rate (mm/s)	0.20	0.24	0.59	1.24	0.85	0.54	0.78	0.89	0.79	1.29	1.20	0.75
Mean horizontal melt-rate (mm/s)	1.30	0.35	0.94	0.53	0.35	0.24	0.37	0.39	0.18	0.27	0.22	0.11
Video observations (time from start +/- 1 s)												
Sand immediately accumulates in cavity?	Y	Y	N	N	N	N	N	N	N	N	N	N
Initial sand movement rapid with no accumulation?	N	N	Y	Y	Y	Y	Y	Y	Y	Y	Y	Y
Sand starts to accumulate to develop sand cap (s)	1	1	3	7	6	8	4	6	7	5	14	
Sand cap established with equilibrium size (s)			7	12	9	13	7	9				
"Shoulders" start to develop at base of sand cap (s)			12	12	15	23	13					
Sand cap becomes unstable (s) and starts to disperse				25	35				15	8	19	
Sand cap persists until end of experiment?	Y	Y?[d]	Y	Y	N	Y	Y	Y	N	N	N	N
Sand caps form transiently, but disperse?	N	N	N	N	N	N	N	N	Y	Y	Y	N
Discrete patches of sand accumulate but no sand cap?	N	N	N	N	N	N	N	N	N	N	N	Y

[a] Temperature in delivery tube measured with K-type thermocouple; sand in reservoir c. 20 °C hotter
[b] CMW = condensate plus meltwater. CMW to sand ratio = (steam condensed + ice melted)/ sand discharged
[c] Ice melt latent heat plus sensible heat of meltwater
[d] View obscured by sand accumulation in cavity

At the start of experiments with added steam (Experiments 3-12), sand appeared to be moving rapidly on the cavity roof without accumulating. A "dimple" formed on the preform roof almost immediately and appeared to be clear of sand and liquid for the first 2-3 seconds. In Experiments 3-8 sand then started to accumulate in the dimple, sand caps began to develop (Figure 6a), grew to an equilibrium size and, in most cases, persisted until the sand supply ceased. Sand was shed radially from the base of the cap and streamed down the sides of the growing cavity. "Shoulders" began to develop on the cavity roof on either side of the base of the sand cap. In Experiments 3 and 4, where the steam to sand ratio was small (0.05 to 0.07), there was very slow (c. 0.1-0.2 mm s^{-1}) vertical melting above the sand cap; most of the melting appeared to be focused on the shoulders, together with horizontal melting of the preform. The shoulders became increasingly pronounced with time (Figure 6b). At the end of Experiments 3 and 4, the shoulders appeared to have bulged slightly above the level of the base of the sand cap; this can be seen on the left hand side of Figure 6c for Experiment 3. With a greater steam to sand ratio of 0.11 to 0.14 in Experiments 5-8, "shoulders" developed at the base of the sand cap (Figure 7d) but these did not become as prominent as those developed in Experiments 3 and 4. In Experiments 5-8 the vertical melt-rate while the sand caps were present was c. 0.4 mm s^{-1}.

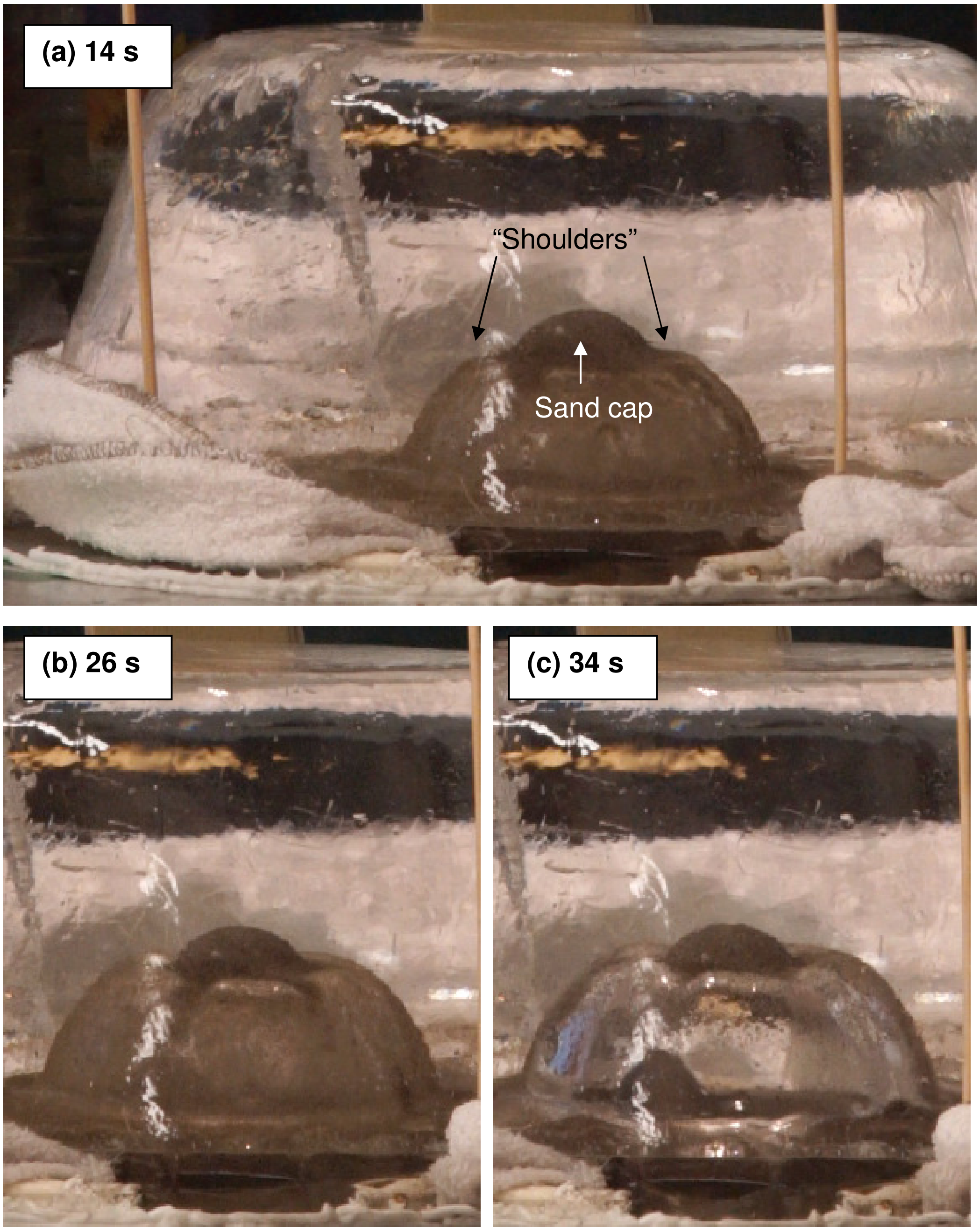

Figure 6. Progressive development of "shoulders" on either side of a stable sand cap was observed with low steam to sand ratios (Experiment 3, with a steam to sand ratio of 0.05, shown here). Times indicated on the images are from the start of the experiment. The height of the ice block is 10 cm.

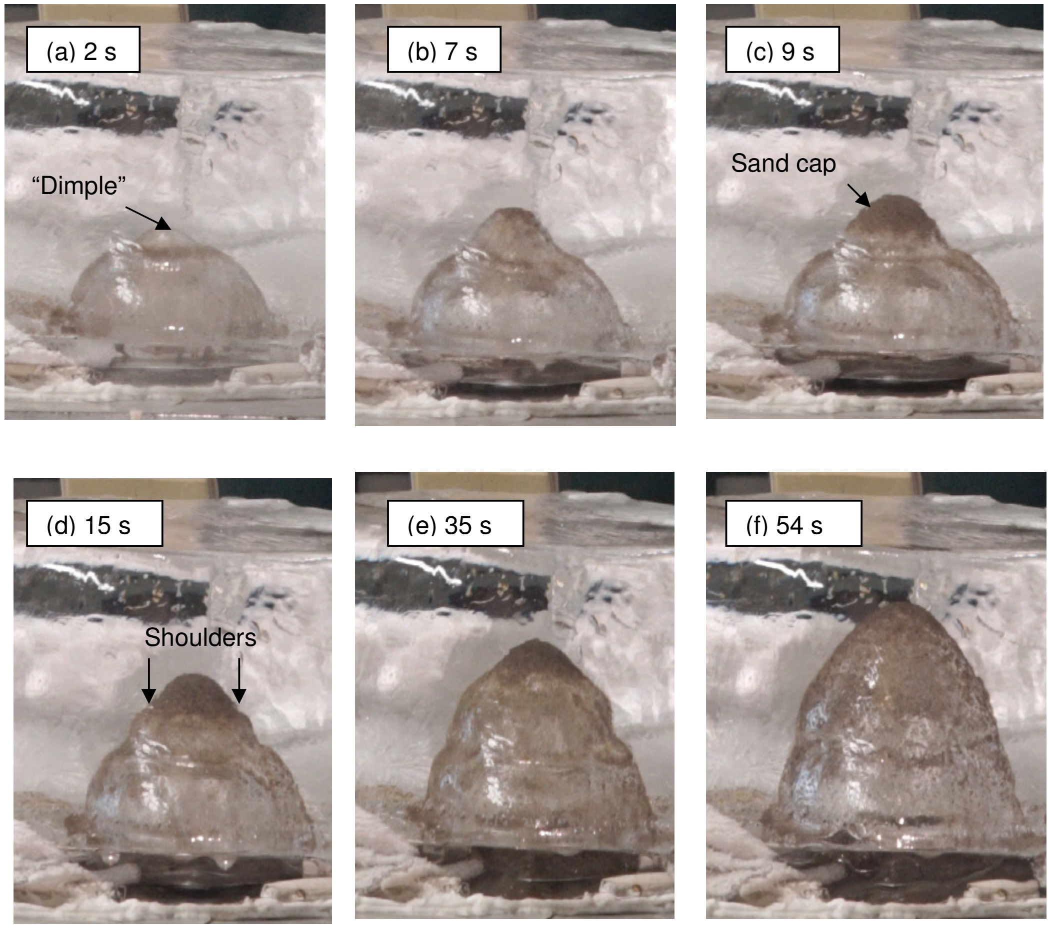

Figure 7. Cavity development with a larger steam to sand ratio is shown in this sequence of images of cavity development during Experiment 5 (steam to sand ratio of 0.11). (**a**) A pronounced "dimple", which appears to be clear of sand and water, develops on the preform roof. (**b**) Sand begins to accumulate in the dimple to develop a sand cap. (**c**) The sand cap reaches a steady state size and sheds sand radially from the base of the cap. (**d**) Shoulders develop at the base of the sand cap. **(e)** The sand cap begins to decrease in size. (**f**) The cavity at the end of the experiment; compare with Figures 5b and 6c. Times indicated on the images are from the start of the experiment. The height of the ice block is 10 cm.

Increasing the steam to sand ratio further (Experiments 9-11, with steam to sand ratios between 0.15 and 0.29) resulted in the development of a sand cap in the dimple that quickly became unstable and dispersed. Sand then appeared to distribute itself evenly over the cavity surface and flowed readily in the liquid water with minimal accumulation of sand in the top of the growing cavity (Figure 8). Occasionally, discrete patches of sand developed but these tended to disperse before they coalesced into an established sand cap. There was maximum vertical melting at 1-1.5 mm s^{-1}, concentrated mainly in the dimple, which widened radially to dominate the cavity. Experiment 12, with the highest steam to sand ratio of 0.78, did not develop sand caps and sand appeared to distribute itself evenly over the cavity surface.

Figure 8. This image, at 26 s after the start of Experiment 10 (steam to sand ratio of 0.20), shows vertical upward melting, discrete sand patches but no accumulation into a sand cap. The height of the ice block is 12 cm.

3.3 Interpretation of experimental results

With no added steam, the small amount of meltwater produced a low mobility slurry of sand and water. Heat transfer from the low mobility slurry during transit on the cavity walls was relatively inefficient; thus hot sand was cooled further by contact with the base of the ice block adjacent to the cavity. Neverthless, the majority (70%+) of the thermal energy in the jet was transferred to the ice.

A small steam to sand ratio produced a slurry that was more mobile but sufficiently immobile to allow a stable sand cap to persist throughout the experiment. Heat transfer from sand to ice was inefficient through the sand cap, so vertical melting was relatively slow. Warm sand slurry flowed along the base of the cap (Figure 9a) and promoted melting of ice adjacent to the base of the cap to produce shoulders in the ice cavity. Heat transfer efficiency from jet to ice was similar to the dry jet (75%).

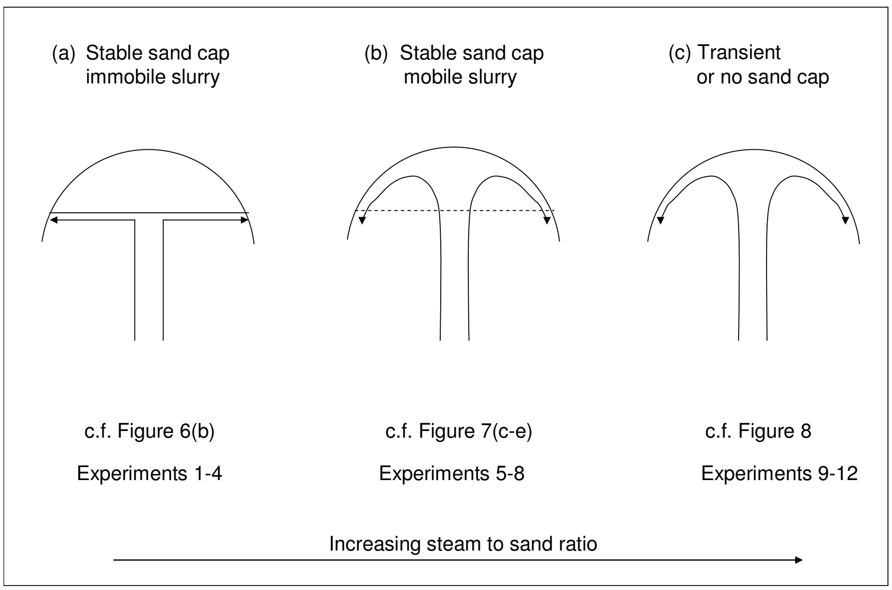

Figure 9. Sequence of diagrams showing the effect of increased steam to sand ratio in the jet on the behavior of sand in the ice cavity during the experiments. **(a)** At the lowest steam to sand ratio the slurry was relatively immobile thus, once a sand cap formed, the sand in the jet was diverted along the base of the sand cap (shown as a solid line) to promote horizontal melting. **(b)** Increased steam to sand ratio resulted in a more mobile slurry so that the sand in the jet could penetrate the base of the sand cap (shown as a dashed line) and flow through the sand cap, increasing vertical melting. **(c)** At the highest steam to sand ratio the slurry was sufficiently mobile to prevent establishment of a sand cap, thus allowing the highest rates of vertical melting.

With a larger steam to sand ratio the sand slurry was more mobile. Vertical melting was much faster, the shoulders were much less prominent and the base of the sand cap was more diffuse. This suggests that sand may have flowed through the sand cap rather than flowing along the base (Figure 9b). Heat transfer efficiency from jet to ice increased to between 85 and 90%.

With the largest steam to sand ratio, the presence of extra water gave the sand slurry a much greater mobility than in previous experiments. Consequently, sand cap formation was transient and any sand accumulated as small patches, allowing more rapid heat transfer between sand and ice and the highest rates of vertical melting (Figure 9c). In Experiment 12 the sand flow rate was very low at 0.5 g s^{-1}; consequently the resulting sand slurry was very dilute and thus mobile. In this experiment vertical melt-rates were probably limited by the availability of hot sand, but heat transfer efficiency between jet and ice was very high at 99%.

We postulate that the sand cap generated in the experiments (Figures 6, 7 and 9) comprised particles bonded by the surface tension of liquid bridges. A significant proportion of pore space was occupied by gas giving a three-phase mixture that had a yield strength and was relatively thermally insulating. Increasing availability of liquid water reduced the proportion of gas phase until the cap lost cohesion as saturation was approached.

The experiments indicate that the mobility of the sand slurry is an important control on the efficiency of heat transfer from the jet and the extent of vertical melting. The results in Table 2 show that, as the steam to sand ratio increased, (1) the proportion of heat in the jet that melted ice and heated meltwater increased, and (2) the meltwater temperature decreased, thus more of the heat was transferred to melt ice. In addition, mean vertical melt-rate increased while mean horizontal melt-rate decreased. The experimental sand cap acted to attenuate ice melting above the buoyant jet. Instead, heat was coupled into the ice away from the impingement footprint of the jet encouraging ice melting over a broader area perpendicular to the jet axis. The presence of a stable particle cap also reduced the overall rapid heat transfer efficiency, but not to a large extent.

Figure 10 explores the relative contributions of vertical and horizontal melting to the development of an ice cavity as the steam to sand ratio varies. Vertical melting is represented by the difference between the final height of the cavity and the initial preform height. Horizontal melting is represented by the difference between the final basal diameter of the cavity and the basal diameter of the preform. Figure 10 shows a trend from predominantly horizontal melting, when sand caps were established for most of an experiment, to predominantly vertical melting as the steam to sand ratio was increased and sand caps were transient or did not form.

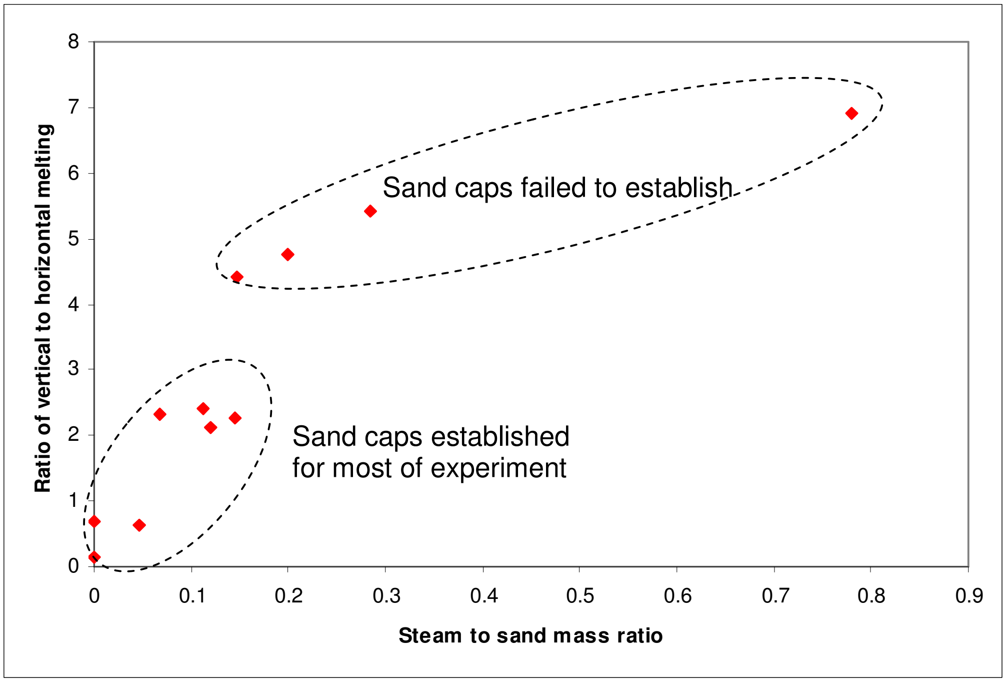

Figure 10. Ratio of vertical to horizontal melting in the ice cavities produced during the experiments versus steam to sand mass ratio. Horizontal melting dominated at low steam to sand ratios when sand caps were established for most of the experiment. At higher steam to sand ratios, when sand caps did not become established, vertical melting dominated. Errors in the ratio of vertical melting to horizontal melting are 10-15% while errors in the steam to sand ratio are 3-6%.

Figure 11 shows the variation of vertical ice-melt with time during two of the experiments. In Experiment 3, with a steam to sand ratio of 0.05, the melt-rate was relatively fast initially, decreased as a sand cap became established (Figure 6) and remained at low rates (0.1-0.2 mm s^{-1}) for the rest of the experiment, when the sand cap insulated the top of the cavity from jet impingement. In Experiment 10, with a steam to sand ratio of 0.2, the melt-rate was initially similar to Experiment 3, but in this case a sand cap did not become established and the melt-rate remained relatively high (1.0-1.5 mm s^{-1}) for the rest of the experiment.

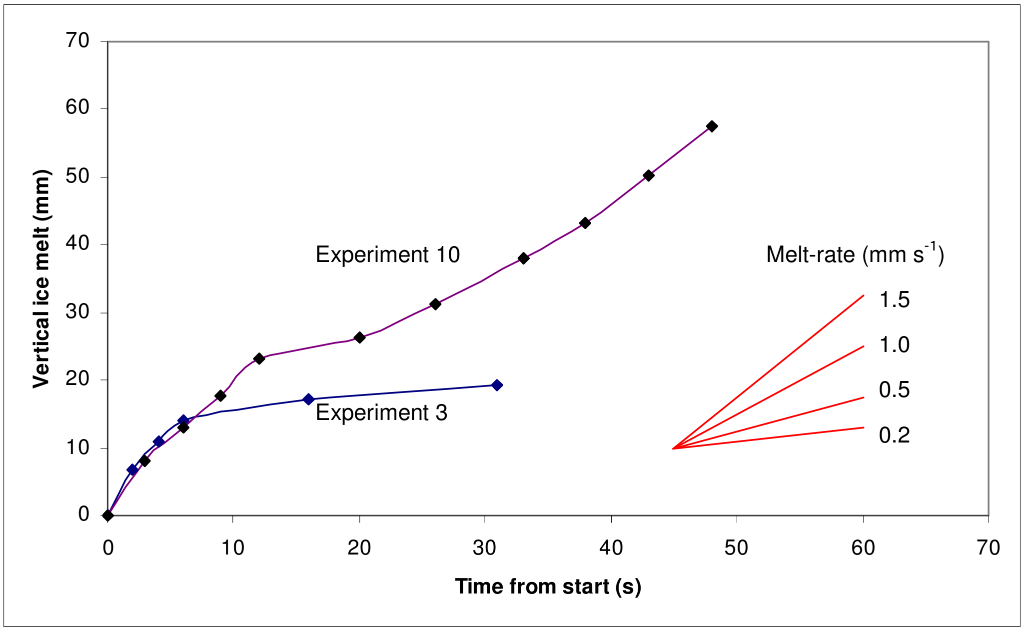

Figure 11. Vertical ice-melt versus time from the start of an experiment for Experiment 3, where a sand cap became established early in the experiment, and for Experiment 10, where a sand cap developed in the initial few seconds of the experiment and then dispersed. The melt-rate at any time may be estimated by comparing the local gradient of the graph for an experiment with the “fan” of melt-rates at the bottom right hand side. Vertical ice-melt is accurate to +/- 1 mm; time from start is accurate to +/- 1 s.

4 Discussion

Sections 2 and 3 describe laboratory experiments in which hot sand impinged on the underside of a block of ice. This section discusses the relevance of the experimental results to subglacial volcanic systems and considers the wider implications by comparing the melt-rates observed in the experiments that are volcanically relevant with melt-rates estimated by other heat transfer mechanisms proposed for subglacial eruptions and with melt-rates inferred from recent eruptions.

4.1 Relevance of the experimental results to subglacial eruptions

4.1.1 Which experiments are volcanically relevant?

In Section 3 we reported the results of a series of experiments in which the steam to sand ratio was varied and we interpreted the range of behaviors observed in terms of the varying mobility of the sand slurry within the growing ice cavity. For sand at a constant temperature we observed that increasing the steam to sand ratio in the jet increased the water to sand ratio in the resulting slurry and the mobility of the slurry. By analogy, we expect that behavior during a subglacial eruption may be determined principally by the water to pyroclast ratio in the slurry on the ice surface of the cavity during the eruption. We determine this ratio below.

In a subglacial eruption, pyroclasts may be produced by a combination of magmatic fragmentation and magma-water interaction in the volcanic conduit. In the former end-member case pyroclasts are at magmatic temperature; in the latter case cooler pyroclasts are accompanied in the eruption jet by steam produced during phreatomagmatism. If the pyroclasts and steam are cooled to the same final temperature, the net effect, in terms of the mass of ice melted and thus water to pyroclast ratio, is the same for both cases. We establish the range of water to pyroclast mass ratios for subglacial eruptions as follows by reference to the case with no magma-water interaction in the conduit and assuming all available heat in the eruption jet is available to melt ice and heat the resulting meltwater.

Consider unit mass of dry (volatile-free) magma with initial temperature T_i, specific heat capacity C_p and associated magmatic steam σ (kg steam/kg dry magma). If, after contact with ice, both magma and magmatic steam cool to a final temperature T_f

below the boiling point then the heat available to melt ice (in J/kg dry magma) is given by:

$$Q_m = C_p\left(T_i - T_f\right) + \sigma\left[C_s(T_i - T_b) + (h_v - C_w T_f)\right] \qquad (1)$$

where C_s and C_w are the specific heat capacities of steam and liquid water respectively and h_v is the enthalpy of steam (relative to liquid water at 0 °C) at the boiling point T_b.

The heat required to melt unit mass of ice and raise the meltwater temperature to T_f is $(L_f + C_w T_f)$ where L_f is the latent heat of fusion of ice. The resulting water to pyroclast mass ratio φ_2 is thus:

$$\phi_2 = C_p \frac{(T_i - T_f)}{(L_f + C_w T_f)} + \sigma \frac{\left[C_s(T_i - T_b) + (h_v - C_w T_f)\right]}{\left(L_f + C_w T_f\right)} + \sigma \qquad (2)$$

where the first term is the contribution from the solid particles and the second and third terms are the contributions from the heat and mass respectively of the associated magmatic steam.

Equation 2 assumes complete thermal equilibration between magma and water and thus represents the maximum water to pyroclast ratios available to control the behavior of the slurry of volcanic ash and water draining from the melting cavity wall during a subglacial explosive eruption. Phreatomagmatic eruptions tend to generate a high proportion of volcanic ash, even for basaltic magmas [*Schopka et al.,* 2006]. Under these conditions, the latent heat of secondary steam couples effectively to the ice surfaces [*Woodcock et al.*, 2015] and the warm ash is thermally coupled to both liquid and gaseous water. In our experiments, at least 70% of the effective jet heat melted ice, with efficiencies potentially as high as 90%. This indicates that the maximum water to particle ratios calculated above could be approached at volcanic scale.

We evaluate Equation 2 for typical basaltic and rhyolitic magmas, assuming the cavity pressure is atmospheric. For basaltic magma with an initial temperature of 1100 °C containing 1 % mass of water, the resulting water to pyroclast mass ratios φ_2 are 2.9 and 3.7 for final temperatures of 20 °C and 0 °C respectively. The corresponding water to pyroclast mass ratios, for a rhyolitic magma initially at 850 °C with 3 % water, are 2.4 and 3.1. In the experiments, where the ratio of steam to sand could be varied independently of sand temperature, the water to sand mass ratio varied from 0.58 to 6.20, spanning the maximum volcanic values. Experiments indicated that a particle cap was only stable where the water to particle ratio was less than approximately 1.6 (Table 2), which is lower than the water to pyroclast ratios available during a subglacial explosive eruption. We conclude that the development of a particle cap in the volcanic case is unlikely; thus the volcanically relevant experiments are those in which stable sand caps did not develop. Experiments 10 and 11 (Table 2) most closely scale to the volcanic case with approximately 20% 'phreatomagmatic' secondary water added and nearly 90% thermal efficiency. However, total particle flux within a jet will change as a function of vent area, suggesting that moving from a centimetre-scale experiment to a metre-scale volcano results in an order 10^4 scale increase in total particle flux. These particles, should they couple into the melt and condensate water, then drain in a film whose thickness and velocity is likely to be scale independent. The increase in drainage area therefore scales with cavity radius suggesting a scale increase of order 300. This suggests that the particle number density at volcanic scale will be order 30 times larger than at experimental scale. These scale considerations are mitigated by evidence [*Gerstmann and Griffith*, 1967; *Anderson et al.*, 1998; *Woodcock et al.*, 2015] that draining condensate and melt films develop troughs and ridges at sub-metre scale that would act to shed the slurry on length scales closer to that of the experiment than the volcanic cavity. Volcanically, the more plume-like nature of the impingement is likely to spread the thermal interaction over a wider area of relatively small local 'cells' of heat transfer that will create a 'rain' of ash-laden liquid droplets within the circulating cavity fluids.

4.2 Wider implications

In the experiments, we observed vertical melt-rates of up to 1.5 mm s^{-1} (Figure 11), equivalent to a heat flux of 500 kW m^{-2} at the ice melting surface, that were produced by a combination of pyroclast-ice heat transfer and steam condensation. Experimentally, specific jet power was a third of that estimated for the Gjálp 1996 eruption (Table 1) suggesting that, volcanically, vertical melt-rates could be higher. However, scaling arguments have suggested that the larger scale volcanic buoyant jet may couple to the ice over proportionately larger areas than for small-scale experiments. Heat fluxes of 1-2 MW m^{-2} are estimated for steam condensation within pressurized, vapor-dominated cavities [*Woodcock et al.*, 2015], but under conditions of atmospheric pressure, and a significant mole fraction of non-condensable gases, estimated heat fluxes are very similar to those found here in the small-scale experiments that mimic the buoyant jet of a warm, wet, phreatomagmatic eruption.

Heat fluxes of 3-5 MW m^{-2} were estimated for two-phase convection within pressurized liquid-dominated cavities [*Woodcock et al.*, 2014], an order of magnitude higher than for particle-laden buoyant jets. In addition, the experimentally determined heat fluxes are much lower than values from recent Icelandic subglacial eruptions, where heat fluxes of 1.2-1.6 MW m^{-2} at the 1996 Gjálp eruption and 3-4 MW m^{-2} at the Eyjafjallajökull summit eruption in 2010 were inferred. In both cases much of the evidence suggests that the subglacial cavities were predominantly filled with liquid water at elevated pressure [*Gudmundsson et al*., 2004; *Magnússon et al*., 2012].

To date there has been no observational evidence for ice-melt by pyroclast-ice heat transfer, although it may have occurred during a minor eruption observed on the slopes of Eyjafjallajökull in 2010 [*Magnússon et al.,* 2012]. However, ice-melt by pyroclast-ice heat transfer is a plausible mechanism during eruptions in water-drained, low pressure cavities. Such cavities may develop on sloping terrain, where ice may be relatively shallow and gravity drainage of meltwater may be promoted. We considered such a subglacial environment in *Woodcock et al.* [2016] in the context of our quantification of steam condensation and radiation transfer from an eruption jet, where heat fluxes of c. 300 kW m^{-2} were demonstrated.

5 Conclusions

(1) A phreatomagmatic eruption in a water-drained, low pressure subglacial eruption cavity was simulated by a jet of hot sand and steam at approximately 300 °C impinging on the underside of a block of ice. A set of experiments with an increasing ratio of steam to sand in the jet showed that the behavior ranged from predominantly horizontal melting with the development of a stable sand cap to predominantly

vertical melting by a mobile slurry of sand and water without sand cap development. The experiments indicate that the mobility of the sand slurry is an important control on the efficiency of heat transfer from the jet and the extent of vertical melting.

(2) Heat balance calculations indicate that the experiments with large steam to sand ratios have water to particle ratios in the range expected for the volcanic situation. These experiments, which showed no development of stable sand caps, are thus the most representative of behavior in the volcanic situation. The experimental sand cap regime, with lower water to particle ratio, is unlikely to develop in the volcanic situation.

(3) Vertical ice melt-rates of 1.5 mm s^{-1} were observed in the experiments. These rates are much smaller than melt-rates inferred from recent Icelandic subglacial eruptions, where cavities are inferred to have remained flooded and at elevated pressure. However, experimental melt-rates are similar to estimates of melt-rates in low pressure cavities by steam condensation in the presence of significant levels of non-condensable gases. Thus pyroclast-ice heat transfer may be an important ice-melt mechanism for subglacial eruptions in drained, low pressure cavities that may develop on sloping flanks of glaciated volcanoes.

Acknowledgements

The data supporting this paper are available as Supporting Information and from http://dx.doi.org/10.17635/lancaster/researchdata/122. We thank two anonymous reviewers for their detailed comments during review which have greatly improved the paper. We also thank the Editor André Revil and the Associate Editor for their comments. We thank Magnus Tumi Gudmundsson, Mike James, Kelly Russell and Steve Sparks for comments on an earlier version of this paper.

References

Anderson, M.H., L.E. Herranz, and M.L. Corradini (1998), Experimental analysis of heat transfer within the AP600 containment under postulated accident conditions, *Nuclear Enginering and Design, 185*, 153-172.

Bird, D.K., G. Gisladottir, and D. Dominey-Howes (2010), Volcanic risk and tourism in southern Iceland: implications for hazard, risk and emergency response, education and training, *Journal of Volcanology and Geothermal Research, 189*, 33-48.

Bonaccorso, A., and S. Calvari (2013), Major effusive eruptions and recent lava fountains: Balance between expected and erupted magma volumes at Etna volcano, *Geophysical Research Letters, 40*, 6069–6073, doi:10.1002/2013GL058291.

Dellino, P., M.T. Gudmundsson, G. Larsen, D. Mele, J.A. Stevenson, T. Thordarson, and B. Zimanowski (2012), Ash from the Eyjafjallajökull eruption (Iceland): fragmentation processes and aerodynamic behavior, *Journal of Geophysical Research, 117*, B00C04, doi:10.1029/2011JB008726.

Gerstmann, J., and P. Griffith (1967), Laminar film condensation on the underside of horizontal and inclined surfaces, *International Journal of Heat and Mass Transfer, 10*, 567-580.

Gudmundsson, M.T. (2003), Melting of ice by magma-ice-water interactions during subglacial eruptions as an indicator of heat transfer in subaqueous eruptions, in *Explosive Subaqueous Volcanism, Geophysical Monograph Series,* vol. 140, edited by J.D.L. White, J.L. Smellie, and D.A. Clague, pp. 61-72, AGU, Washington, D.C.

Gudmundsson, M.T. (2005), Subglacial volcanic activity in Iceland, in *Iceland: Modern processes, Past Environments, Developments in Quaternary Science,* vol. 5*,* edited by C.J. Caseldine et al., pp. 127-151, Elsevier, Amsterdam.

Gudmundsson, M.T., F. Sigmundsson, H. Bjornsson, and T. Hognadottir (2004), The 1996 eruption at Gjálp, Vatnajökull ice cap, Iceland: efficiency of heat transfer, ice deformation and subglacial water pressure, *Bulletin of Volcanology, 66*, 46-65.

Harris, A.J.L., L. Gurioli, E.E. Hughes, and S. Lagreulet (2012), Impact of the Eyjafjallajökull ash cloud: a newspaper perspective, *Journal of Geophysical Research, 117*, B00C08, doi:10.1029/2011JB008735.

Höskuldsson, A., and R.S.J. Sparks (1997), Thermodynamics and fluid dynamics of effusive subglacial eruptions, *Bulletin of Volcanology, 59*, 219-230.

Incropera, F.P., and D.P. DeWitt (1996), *Introduction to Heat Transfer*, John Wiley, New York.

Krumbholz, M., C.F. Hieronymus, S. Burchardt, V.R. Troll, D.C. Tanner, and N. Friese (2014), Weibull-distributed dyke thickness reflects probabilistic character of host-rock strength, *Nature Communications, 5*, 3272, doi:10.1038/ncomms4272.

Magnússon, E., M.T. Gudmundsson, G. Sigurdsson, M.J. Roberts, F. Höskuldsson, and B. Oddsson (2012), Ice-volcano interactions during the 2010 Eyjafjallajökull eruption, as revealed by airborne radar, *Journal of Geophysical Research*, 117, B07405, doi:10.1029/2012JB009250.

Paterson, W.S.B. (1994), *The Physics of Glaciers*, Butterworth-Heinemann, Oxford.

Papanicolaou, P.N. and J.E. List (1988), Investigations of round vertical turbulent buoyant jets, *Journal of Fluid Mechanics, 195*, 341-391.

Raju, N. and E. Meiburg (1995), The accumulation and dispersion of heavy particles in forced two-dimensional mixing layers. Part 2: the effect of gravity, *Phys. Fluids, 7*, 1241-1264.

Rogers, G.F.C., and Y.R. Mayhew (1980), *Thermodynamic and Transport Properties of Fluids (SI Units),* Blackwell Publishing, Oxford.

Schopka, H.H, M.T. Gudmundsson, and H. Tuffen (2006), The formation of Helgafell, southwest Iceland, a monogenetic subglacial hyaloclastite ridge: Sedimentology, hydrology and volcano–ice interaction, *Journal of Volcanology & Geothermal Research, 152*, 359-377.

Spampinato, L., S. Calvari, C. Oppenheimer, and L. Lodato (2008), Shallow magma transport for the 2002-3 Mt. Etna eruption inferred from thermal infrared surveys, *Journal of Volcanology and Geothermal Research, 177,* 301-312.

Stevenson, J.A., J.S. Gilbert, D.W. McGarvie, and J.L. Smellie (2011), Explosive rhyolite tuya formation: classic examples from Kerlingarfjöll, Iceland, *Quaternary Science Reviews, 30,* 192-209.

US Department of the Interior (2007), The Eruption of Kilauea 1959-1960 Chapter 3, (available in Youtube at http://www.youtube.com/watch?v=aa8Wr6xZPYI - accessed 14 January 2016).

Wilson, L., and J.W. Head (2002), Heat transfer and melting in subglacial basaltic volcanic eruptions: implications for volcanic deposit morphology and meltwater volumes, in *Volcano-Ice Interaction on Earth and Mars,* edited by J.L. Smellie and M.G. Chapman, *Geological Society Special Publication, 202*, 5-26.

Woodcock, D.C. (2016). Magma-ice heat transfer in subglacial volcanism. Ph.D. thesis, Lancaster Environment Centre, Lancaster University, UK.

Woodcock, D.C., S.J. Lane, and J.S. Gilbert (2014), Ice-melt rates in liquid-filled cavities during explosive subglacial eruptions, *Journal of Geophysical Research: Solid Earth, 119*, doi:10.1002/2013JB010617.

Woodcock, D.C., J.S. Gilbert, and S.J. Lane (2015), Ice-melt rates by steam condensation during explosive subglacial eruptions, *Journal of Geophysical Research: Solid Earth*, *120*, doi:10.1002/2014JB011619.

Woodcock, D.C., S.J. Lane, and J.S. Gilbert (2016), Ice-melt rates during volcanic eruptions within water-drained, low pressure subglacial cavities, *Journal of Geophysical Research: Solid Earth,* 121, doi**:** 10.1002/2015JB012036.

Woodhouse, M.J., A.J. Hogg, J.C. Phillips, and R.S.J. Sparks (2013), Interaction between volcanic plumes and wind during the 2010 Eyjafjallajökull eruption, Iceland, *Journal of Geophysical Research: Solid Earth, 118,* 92–109, doi : 10.1029/2012JB009592.